CHEMISTRY OF MATERIALS

Article

pubs.acs.org/cm

Interface Stability in Solid-State Batteries

William D. Richards,[†] Lincoln J. Miara,[‡] Yan Wang,[†] Jae Chul Kim,[†] and Gerbrand Ceder*[,†,¶,§]

[†]Department of Materials Science and Engineering, Massachusetts Institute of Technology, Cambridge, Massachusetts 02139, United States

[‡]Samsung Advanced Institute of Technology - USA, 255 Main Street, Suite 702, Cambridge, Massachusetts 02142, United States

[¶]Department of Materials Science and Engineering, University of California, Berkeley, California 94720, United States

[§]Materials Sciences Division, Lawrence Berkeley National Laboratory, Berkeley, California 94720, United States

Supporting Information

ABSTRACT: Development of high conductivity solid-state electrolytes for lithium ion batteries has proceeded rapidly in recent years, but incorporating these new materials into high-performing batteries has proven difficult. Interfacial resistance is now the limiting factor in many systems, but the exact mechanisms of this resistance have not been fully explained - in part because experimental evaluation of the interface can be very difficult. In this work, we develop a computational methodology to examine the thermodynamics of formation of resistive interfacial phases. The predicted interfacial phase formation is well correlated with experimental interfacial observations and battery performance. We calculate that thiophosphate electrolytes have especially high reactivity with high voltage cathodes and a narrow electrochemical stability window. We also find that a number of known electrolytes are not inherently stable but react in situ with the electrode to form passivating but ionically conducting barrier layers. As a reference for experimentalists, we tabulate the stability and expected decomposition products for a wide range of electrolyte, coating, and electrode materials including a number of high-performing combinations that have not yet been attempted experimentally.

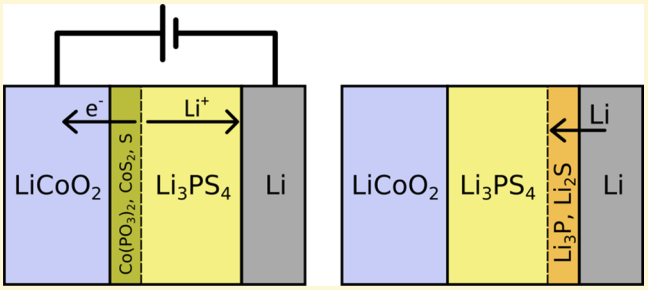

INTRODUCTION

Solid-state electrolytes have the potential to dramatically improve safety and performance of state-of-the-art battery technology. The high energy density and long cycle life of lithium-ion batteries has led to their adoption in all manner of technologies, but serious safety concerns still exist due to their use of flammable organic solvent electrolytes. This is especially problematic for grid-scale storage and transport applications including aircraft and automobiles. Solid-state ionic electrolyte materials are a viable nonflammable alternative, would enable novel device geometries to improve packing efficiency of the cells, and have the potential to improve cycle life and enable higher voltage cathodes.[1] By suppressing dendrite formation, solid electrolytes may also allow the use of metal anodes which would increase energy density considerably. Development of Li-ion solid electrolytes has proceeded rapidly in recent years, with the conductivity of some systems even approaching and surpassing that of liquid electrolytes. Room temperature conductivities of around 1 mS cm^{-1} have been shown in NASICON-type oxides[2−4] and lithium garnets.[5−7] These systems typically require high synthesis temperatures[8] and cosintering to obtain good contact between the electrode and electrolyte,[9] which is important for battery performance.[10,11] New thiophosphate materials based on Li_3PS_4[12] have recently emerged as a novel class of superionic conducting materials with even higher conductivities and whose mechanical properties allow better physical contact with electrodes. These include $Li_{10}GeP_2S_{12}$ (LGPS), with a conductivity of 12 mS cm^{-1} at room temperature,[13] and $Li_7P_3S_{11}$, a glass-ceramic with a room temperature conductivity of 27 mS cm^{-1}.[14] Less expensive versions of LGPS where Ge is replaced by Sn or Si have also been predicted[15] and synthesized.[16−19]

Despite this progress in achieving high bulk conductivity, the rate capability of most all-solid-state cells, particularly those employing high-voltage oxide cathodes, remains poor.[20,21] This is typically ascribed to high internal resistance at the interfaces, but the exact mechanisms by which this resistance builds have been difficult to ascertain experimentally. Chemical incompatibility, electrochemical reaction, and mechanical issues may all play a role in degrading battery performance. Coating the electrodes with an oxide barrier layer has been necessary to suppress development of extreme interfacial resistance and enable high-rate cycling,[13,16,22,23] but many of these cells still see significant degradation after relatively few cycles. The future of solid-state batteries depends on engineering better interfaces to allow high rate capability and extended cycle life in this new generation of batteries. The experimental investigation of interface reactions is tedious as accessing the interface between

Received: October 20, 2015
Revised: December 2, 2015
Published: December 7, 2015

DOI: 10.1021/acs.chemmater.5b04082
Chem. Mater. 2016, 28, 266−273

two solids is difficult and the reaction layers are often only a small fraction of the total solids. For this reason, a predictive modeling approach that formally includes the chemical and electrochemical driving force is highly valuable.

To improve understanding of the causes of interfacial resistance in these systems, we develop in this work a methodology to evaluate the thermodynamic stability of battery interfaces and use it to explain experimentally observed trends. We find that the bulk thermodynamic driving force for reaction between the electrolyte and cathode is a good proxy for interfacial stability and that this contribution to the reaction energy dominates the effects of interfacial energy. We apply our methodology over a broad range of cathode/electrolyte combinations and suggest new strategies for improving device performance. These calculations require only basic thermodynamic data for the electrolytes, cathodes, and possible decomposition products. To obtain this starting data, we leverage the scalability and transferability of Density Functional Theory (DFT) calculations to augment available experimental values. This enables the examination of a wide range of cathode and electrolyte combinations including materials whose thermodynamic properties have not yet been determined experimentally while retaining the accuracy of experimental data in systems where this data is available.

Results of the bulk thermodynamic calculations explain the poor performance seen in many solid-state battery systems, and the generalization of the observed trends leads to design rules for constructing new battery systems. We find that the chemical composition of electrode and electrolyte phases is the primary determinant of interfacial stability but that the performance of these interfaces can be improved by engineering systems where the decomposition phases are passivating (electronically insulating) but still ionically conductive. For example, LiPON,[24] one of the few commercialized solid electrolytes, is calculated to be unstable against a lithium metal anode but forms an ionically conducting passivation layer in situ. In particular, the choice of anion is the most critical factor determining the high voltage stability limit. When paired with high voltage cathodes, thiophosphate electrolytes have a high driving force for reaction to form ionically insulating barrier layers, explaining the high internal resistance seen experimentally. We also identify a number of potentially high performance cathode/solid-electrolyte combinations which have yet to be attempted experimentally. These results are also useful for suggesting combinations of electrolytes, one stable against the anode and one against the cathode, to widen the effective stability window.

METHODS AND RESULTS

The design of solid-state electrolyte materials is challenging due to the extreme conditions they experience in contact with both the anode and cathode. To evaluate interfacial stability we proceed in two stages. We first evaluate the electrochemical stability of the electrolyte by itself by subjecting it to Li chemical potentials (μ_{Li}) typically observed at the anode or cathode. We then extend this model allowing chemical reaction between the electrolyte and electrodes. All of these calculations consider the reaction energy of the bulk phases as the contribution of the actual interfacial energy is relatively small. For example, considering an upper bound for the change in surface energy of 0.5 J m^{-2} with an atomically thin interfacial product, the contribution to the total energy remains only ~100 meV per atom, which we will show is small compared to the bulk driving forces in most relevant systems.

Stability versus Lithium Potential. High energy density batteries necessarily have anodes and cathodes with very different lithium electrochemical potential. We consider first the effects of subjecting the electrolyte to these extreme lithium potentials, without allowing other reactions between the electrolyte and the anode or cathode material. The stability window is determined by the voltages at which lithium is extracted from the electrolyte to form a Li-deficient decomposition layer between the electrolyte and the cathode (Figure 1a, anodic stability) and at which lithium is inserted into the electrolyte, reducing another species and forming a Li-reduced decomposition layer (Figure 1b, cathodic stability).

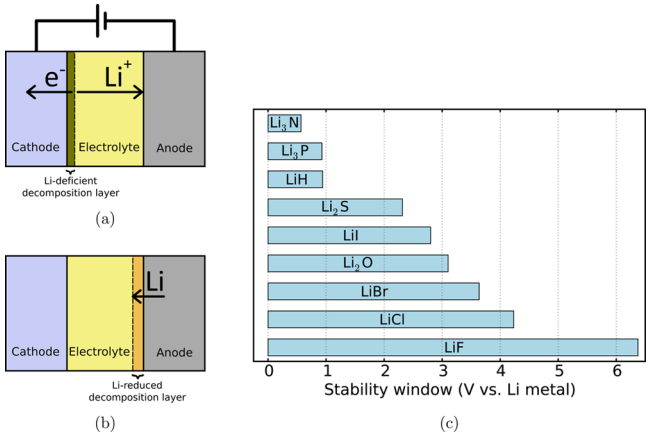

Figure 1. Schematic of a full cell showing a) decomposition of the electrolyte at the cathode/electrolyte interface during charging and b) reduction of the electrolyte by the lithium metal anode. c) Electrochemical stability ranges of lithium binary compounds. Where available, these ranges are computed from experimental thermodynamic data.

For each considered electrolyte, we calculate the range of μ_{Li} over which it is stable by constructing the relevant 0 K grand potential phase diagrams. We consider the grand potential Φ, the characteristic state function of the grand canonical ensemble,[25] for systems open to Li at applied voltages between 0 and 7 V vs Li/Li^+ (μ_{Li} between 0 and −7 eV vs Li metal) according to eq 1, in which $E[c]$ is the enthalpy and $n_{Li}[c]$ is the lithium concentration of composition c, and μ_{Li} is the lithium chemical potential. Phase diagrams are constructed using a database of DFT computed bulk energies of materials with crystal structures obtained from the Inorganic Crystal Structure Database (ICSD)[26] and those generated by applying data-mined chemical substitutions.[27] In general, all known crystalline compounds in a given chemical space are included in this database. Similar data sets can be found online as part of the Materials Project.[28]

$$\Phi[c, \mu_{Li}] = E[c] - n_{Li}[c]\mu_{Li} \quad (1)$$

For any lithium potential μ_{Li}, we then find the resulting stable structures by computing the lower convex hull of Φ in composition space, similar to the approach taken in earlier work.[29] In general, the convex hull is formed by the set of ground state phases in a composition diagram. For any composition, the lowest energy is achieved by a linear combination of these phases. Compounds that are on the convex hull in Φ-composition space are stable in contact with a lithium reservoir at μ_{Li} and cannot lower their energy by decomposition or exchange of Li with the reservoir. Known electrolyte materials that DFT calculates to be metastable at 0 K, e.g. $Li_{10}GeP_2S_{12}$, are placed exactly on the convex hull (i.e., their formation energy from the nearby phases is set to 0) for the stability and reaction energy calculations to account for the small changes in free energy when going from 0 K to elevated temperature. For each structure, we find the range of μ_{Li} over which it is present on the convex hull and therefore stable. As a simple example, the stability ranges for common ionic lithium binary materials are shown in Figure 1c. In all of these

DOI: 10.1021/acs.chemmater.5b04082
Chem. Mater. 2016, 28, 266−273

binary materials, the anion is fully reduced so further reaction with lithium metal cannot occur, and they are therefore stable down to 0 V. At voltages above the stability window, lithium is extracted from these materials yielding the oxidized anion, shown schematically in Figure 1a. These results are in good agreement with the conventional understanding that the halide anions are the most stable at high potential, and materials such as sulfides, nitrides, and phosphides display low anodic limits.

To evaluate the stability of technologically relevant electrolytes, we construct grand potential phase diagrams for a broad range of known solid-electrolyte chemistries using the pymatgen software package.[30] To obtain bulk energies, we employ DFT within the Projector Augmented Wave (PAW) formalism[31] using the generalized gradient approximation[32] to the exchange-correlation energy as implemented in the Vienna ab initio simulation package (VASP)[33] to calculate the formation energy of each electrolyte from the nearest phases present in the NIST-JANAF[34] or Kubaschewski[35] thermochemical tables or from the elements. A cutoff energy of 520 eV and a k-point grid of at least $500/n_{atoms}$ was used for all calculations. We apply the mixing scheme of Jain et al.[36] to combine generalized gradient approximation (GGA) calculations with/without the rotationally invariant Hubbard (+U) correction[37,38] to properly treat insulators and metals. The nearest phases are uniquely defined as those that define the Gibbs triangle (the low energy facet) containing the desired composition in the phase diagram. This phase diagram is generated using only materials for which we have the experimental formation energy, using the DFT computed energies to determine the convex hull. As an example, to calculate the formation energy of $LiYF_4$, a compound whose formation energy is not present in the experimental tables, we use DFT to calculate the energy of the reaction $LiF + YF_3 \rightarrow LiYF_4$ and add the experimental formation energies of LiF and YF_3. This method results in a more accurate formation energy than computing the reaction from the elements since DFT reaction energies have improved accuracy when considering the energetics of systems in which the oxidation state of ions is unchanged.[39] For Li_3PS_4 and similar materials, where the formation energy of Li_2S is present in the thermochemical tables but P_2S_5 is not, we use DFT to calculate the energy of the reaction $3Li_2S + 2P + 5S \rightarrow 2Li_3PS_4$. When possible, such as for $LiAlO_2$, this strategy results in using the experimentally determined formation energy directly. By using experimental energies as much as possible and supplementing them with DFT calculated formation energies when no thermochemical data is available, we maximize our predictive capability.

The calculated stability ranges for common solid-electrolyte materials are shown in Figure 2, with the limiting anodic and cathodic reactions listed in Supporting Information Table S2. In a typical battery, the electrolyte must be stable at lithium potentials between the anode chemical potential (close to 0 eV/atom vs lithium metal) and that set by the cathode (typically around −4 eV/atom for a layered oxide). We find that the anodic stability is determined primarily by the stability window of the related binary, or in the case of mixed anion materials, by that of the least stable related binary material, e.g. the anodic stability of Li_6PS_5Cl is determined primarily by the stability of Li_2S. This phenomenon is explained by considering the pathway of decomposition first to the Li_nX (n = 1, 2, 3, X = anion) binary and resulting phase equilibrium and then dissociation of this binary to extract lithium. According to this two step process, any removal of lithium from the electrolyte must overcome both the formation energy of Li_nX and the energy of mixing with the other binary materials. The energy of mixing widens the electrochemical window over which the electrolyte is stable. In most cases this mixing energy is small and the anodic limit is close to that of the binary, but materials with strongly bound polyanions such as the phosphates and $LiBH_4$ have much wider stability windows since extraction of Li must be accompanied by the dissociation of the polyanion. The exceptions to this rule are those electrolytes that can lose lithium by oxidation of another of their components: e.g. oxidation of Mn^{2+} in Li_2MnBr_4. Figure 2 also shows the expected trend of increasing anodic stability with increasing anion electronegativity.

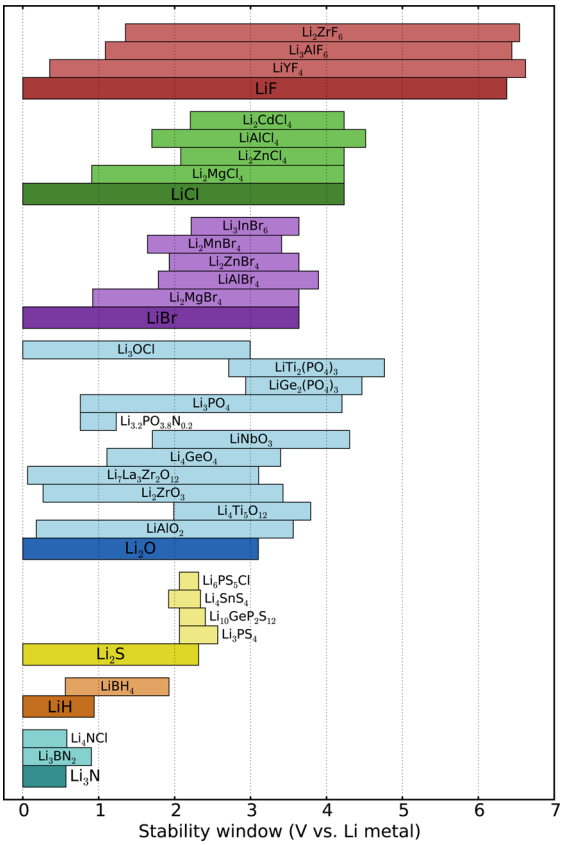

Figure 2. Electrochemical stability ranges of various electrolyte materials grouped by anion, with corresponding binary for comparison. The high-voltage stability of these materials is determined primarily by the anion. The predicted anodic and cathodic reactions that determine these stability windows are listed in Supporting Information Table S2.

In some cases, the stability windows of the electrolyte do not need to extend to the voltages of the anode and cathode. Li_3PS_4, Li_3PO_4, and LiPON are predicted to be unstable against Li-metal from our calculations, but these materials are known experimentally to form a stable interface.[24,40] Table S1 shows that at this interface, a layer of Li_2S/Li_2O and Li_3P is expected to form. Li_3P is a known ionic conductor[41] and so can passivate the decomposition reaction and result in a stable interface still able to conduct lithium. In fact, recent experimental work[42] has observed formation of these passivating products at the interface between a LiPON electrolyte and lithium metal anode. Similarly, our calculations predict passivating phases to extend the anodic stability of LiPON to higher voltages. Above 1.2 V, we calculate decomposition to Li_3PO_4 and Li_2PO_2N.[43] This crystalline LiPON phase has a wider voltage stability window but will further decompose to yield $Li_4P_2O_7$ above 2.75 V, in agreement with the proposed decomposition reaction mechanism of ref 24.

Stability in Contact with Electrodes. The μ_{Li} stability window yields great insight into the performance of an electrolyte in battery systems but does not consider the more complex reactions that may occur between electrolyte and cathode. At the interface between two phases, there is the possibility of reaction to form an intermediate phase or equilibrium of intermediate phases. We now extend the model to investigate the driving forces for such reactions. Since the reaction can consume arbitrary amounts of either phase, we consider the energy of all possible reactions of the form $xc_a + (1 - x)c_b \rightarrow c_{equil}$ where c_a and c_b are the compositions of the two phases in contact, c_{equil} the low energy phase equilibrium determined from the phase diagram, and x a mixing parameter which can vary between 0 and 1. We calculate the reaction of this form with the highest driving force, given by eq 2. In this equation, the function $E_{pd}[c]$ describes the energy of

DOI: 10.1021/acs.chemmater.5b04082
Chem. Mater. 2016, 28, 266−273

the ground state structure or phase equilibrium at composition c determined from the phase diagram. Essentially, this approach finds the products that form with the largest driving force when combining two materials.

$$\Delta E[c_a, c_b] = \min_{x\in[0,1]}\{E_{pd}[xc_a + (1-x)c_b] - xE[c_a] - (1-x)E[c_b]\} \quad (2)$$

To illustrate the approach of eq 2, we consider first a relatively simple system: an interface of Li_2S with $ZnCl_2$. The calculated quaternary phase diagram is shown in Figure 3a. The products of the ground state structure or phase equilibrium at composition c and lithium chemical potential μ_{Li}, as determined from the grand-potential phase diagram (eq 3). We apply the lithium potential determined by the computed average cathode voltage. During cycling, the lithium chemical potential is a function of depth of discharge, but this effect on the reaction energy is small. Because the system is open to Li, reaction energies are normalized by the number of non-Li atoms. The resulting expression (eq 4) is the change in the grand potential of the interfacial region from allowing the electrolyte to equilibrate with the external lithium potential and react with the cathode and determines the interfacial stability as a function of μ_{Li}.

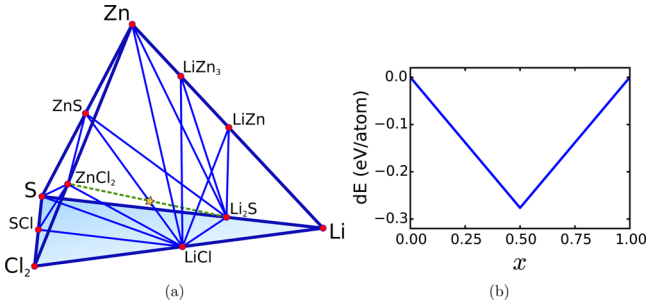

Figure 3. a) Quaternary Li−Zn−S-Cl phase diagram, with stable phases labeled. The reaction vector between $ZnCl_2$ and Li_2S has been marked with a dotted green line, with a star marking the low energy equilibrium at the intersection of the $ZnCl_2$−Li_2S and LiCl-ZnS tielines. b) Energy of the reaction $xZnCl_2 + (1\text{-}x)Li_2S \rightarrow c_{equil}$ as a function of x. The maximum reaction energy is for the complete reaction $ZnCl_2 + Li_2S \rightarrow 2LiCl + ZnS$.

mixing reaction can lie anywhere between Li_2S and $ZnCl_2$. The resulting reaction energies are obtained from the phase diagram and plot as a function of the mixing parameter x in Figure 3b. The interface is not thermodynamically stable and will react to form the lower energy equilibrium of 2LiCl + ZnS with a driving force of 0.27 eV $atom^{-1}$. In contrast, an interface between LiCl and ZnS is predicted to be thermodynamically stable, which can be immediately seen from the presence of a tieline connecting those phases in Figure 3a.

In battery conditions, the interface system is open to lithium. We adapt eq 2 to account for this by replacing $E_{pd}[c]$ and $E[c]$ with their corresponding quantities under the grand potential, $\Phi_{pd}[c, \mu_{Li}]$ and $\Phi[c, \mu_{Li}]$. Similar to $E_{pd}[c]$, $\Phi_{pd}[c, \mu_{Li}]$ describes the energy of the

$$\Phi_{pd}[c, \mu_{Li}] = \min_{n_{Li}}\{E_{pd}[c + n_{Li}] - n_{Li}[c]\mu_{Li}\} \quad (3)$$

$$\Delta\Phi[c_{cathode}, c_{electrolyte}, \mu_{Li}] = \min_{x\in[0,1]}\{\Phi_{pd}[xc_{cathode} + (1-x)c_{electrolyte}, \mu_{Li}] - x\Phi[c_{cathode}, \mu_{Li}] - (1-x)\Phi[c_{electrolyte}, \mu_{Li}]\} \quad (4)$$

The magnitude of $\Delta\Phi$ ultimately governs the thermodynamic stability of the interface, but we can obtain a deeper understanding of the two contributions to this value by comparing it to that of $\Delta\Phi_{no\ mixing}$ (eq 5), in which we do not allow mixing of the cathode with the electrolyte by enforcing $x = 0$ in eq 4. $\Delta\Phi_{no\ mixing}$ measures only the reaction energy from equilibration with the external lithium reservoir and is therefore correlated with the distance between the cathode voltage and the stability range of the electrolyte shown in Figure 2. By this definition, the magnitude of $\Delta\Phi$ is guaranteed to be at least as large as $\Delta\Phi_{no\ mixing}$. In systems where $\Delta\Phi$ and $\Delta\Phi_{no\ mixing}$ are approximately equal, the driving force from decomposition arises mainly from extraction or insertion of lithium as opposed to reaction with the other components of the electrode.

$$\Delta\Phi_{no\ mixing}[c_{electrolyte}, \mu_{Li}] = \Phi_{pd}[c_{electrolyte}, \mu_{Li}] - \Phi[c_{electrolyte}, \mu_{Li}] \quad (5)$$

Results of calculations of $\Delta\Phi$ and $\Delta\Phi_{no\ mixing}$ for various cathode/electrolyte combinations are shown in Figure 4. The results of these calculations for all of the electrolytes in Figure 2 are available in the Supporting Information as Figures S1−S7. Generally, electrolyte materials that are predicted to be stable at the cathode voltage show low reaction energies as they come entirely from the mixing of cathode and electrolyte compositions and do not involve redox activity. Thiophosphate materials tend to have high reaction energies, a large part as a result of applying the cathode lithium potential but also from strong reactions between the PS_4 groups and oxide cathodes to form

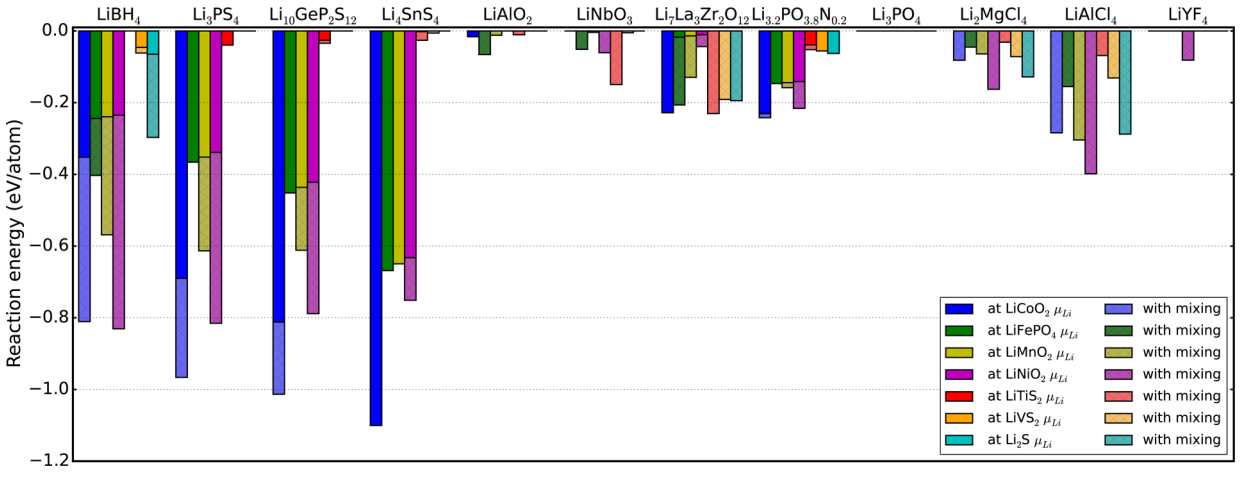

Figure 4. Reaction energies for the interfaces of a selection of cathode/electrolyte combination at μ_{Li} corresponding to the average cathode voltage. Energies are given both for the energy of the lithium extraction only (no mixing) and for energy of cathode/electrolyte mixing open to lithium. Combinations with decomposition energies close to zero are expected to form stable interfaces. The results of these calculations for all of the electrolytes in Figure 2 are available in the Supporting Information as Figures S1−S7.

DOI: 10.1021/acs.chemmater.5b04082
Chem. Mater. 2016, 28, 266−273

PO_4 groups and transition metal sulfides. The details of these predicted reactions can be found in the Supporting Information Table S2. For the sulfide electrolytes, the largest reaction energies are with the layered $LiCoO_2$ and $LiNiO_2$ due to their high voltage and oxygen chemical potential, but even against $LiFePO_4$ these electrolytes are unstable. In contrast, the oxide materials are considerably more stable.

In systems which have been attempted experimentally, there is good correlation between cycle life and the magnitude of the calculated decomposition energy. Most notably, the stability range for the thiophosphate electrolytes in Figure 2 are very narrow, with predicted stability only between 2 and 2.5 V vs Li metal. In these systems, including Li_4SnS_4[44] or $Li_{10}GeP_2S_{12}$[13,16] electrolytes, oxide coatings on the cathode and high voltage (low μ_{Li}) anode materials, e.g. indium metal, must be used. Additionally, recent work[45] has shown that $Li_{10}GeP_2S_{12}$ can be used as an anode, cathode, and electrolyte in a battery, with carbon added to increase the electrical conductivity of the electrode materials.

A few full-cell configurations have been shown experimentally to require minimal overpotential and to exhibit good cycle life. A cell utilizing $LiTiS_2$ cathode with $Li_2S-P_2S_5$ electrolyte[46] has been shown to be relatively stable over many cycles even at elevated temperatures. Our calculations predict only a small driving force for insertion of lithium into the Li_3PS_4 electrolyte (chemically very similar to a $Li_2S-P_2S_5$ glass) due to the very low voltage of the cathode. Good performance has also been achieved in a wide variety of cells using a LiPON electrolyte,[1,47] which we calculate to be stabilized by the formation of a passivating layer of Li_3PO_4 at high voltages. This is another example of where the decomposition reaction (see Table S1) must be examined for passivating products that retain Li-ion conductivity.

This thermodynamic analysis can also be applied to find mitigating solutions in systems where we predict cathode/electrolyte combinations to react. Typically cathode coatings such as $Li_4Ti_5O_{12}$,[22,23] $LiAlO_2$,[16] $LiTaO_3$,[22] or $LiNbO_3$[13,22] are used at the cathode-electrolyte interface. Figures 2 and 4 show clearly why such a barrier layer is effective - the stability window of these materials is much wider than any of the sulfide materials, and all of these are stable at oxide cathode voltage.

DISCUSSION

Interfacial stability is a key problem for solid-state battery devices. In this paper we have developed the foundation of a predictive approach to establish the electrochemical and chemical reactivity between electrodes and electrolytes. Our thermodynamic analysis of electrolyte materials enables an understanding of the processes governing interfacial stability and is easily scalable to examine electrolyte/electrode combinations across a wide range of chemical systems. In this work, we combine DFT with experimental data to expand the thermodynamic data available for our analysis. The same methods can be applied to purely experimental thermochemistry data in systems where it is available.

Though our methodology does not consider explicitly the kinetics of interfacial layer formation, these are intimately related to the bulk thermodynamics. Typically, solid-state reaction rates are limited by either diffusion or nucleation kinetics. For the formation of a thin interfacial layer, the diffusion distance for all reacting species is very small and hence the diffusion time constant is expected to be short. The heterogeneous nucleation rate of the interfacial layer is determined by the free energy of the critical nucleus $\Delta G^* = 16\pi\gamma^3/(3\Delta G^2)\cdot S(\theta)$, where ΔG is the change in energy of the bulk, γ is the interfacial energy, and $S(\theta)$ is a shape factor less than 1.[48] Since incoherent interfacial energies do not vary much among ionic solids, for an interface to be kinetically stabilized by a nucleation barrier it must have a small reaction energy.

One major area of battery research is the use of newly developed thiophosphate materials having extremely high lithium conductivity in conjunction with relatively high voltage cathodes. These interfaces have two pathways leading to device failure. First, considering only the lithium chemical potentials experienced by the electrolyte shows that attempting to charge a typical oxide cathode is likely to lead to the formation of a passivating but highly resistive sulfur layer by lithium extraction. Second, in contact with an oxide cathode, mixing of the cathode and electrolyte is to be expected due to the high stability of the phosphate anion and Li_3PO_4 phases. This is in good agreement with experimental observation of P and Co transport across the interface in a $LiCoO_2/Li_2S-P_2S_5$ battery.[49]

There has been speculation that the interfacial resistance is caused by a space charge region with Li segregation into the cathode decreasing conductivity.[23] While this segregation is certainly possible and is likely to occur to some extent, it would result in an increase in conductivity by increasing the number of charge carriers. Our calculations suggest that complete breakdown of the electrolyte including oxidation of S^{2-} to form a blocking layer is more likely at the chemical potentials of typical oxide cathode materials. Commonly, cyclic voltammetry is used to evaluate and report electrolyte stability. Somewhat surprisingly given the inherent stability limitations of the sulfide materials, extremely wide stability windows have been reported, in some reports extending as high as 10 V vs Li metal.[13,14,50] This may be caused by a thin layer of oxidized, lithium deficient, electrolyte at the electrode, for example elemental sulfur in systems containing thiophosphate electrolytes. Such an interfacial layer will significantly impede lithium mobility, so CV curves should be augmented by Li transport measurements at these high voltages to confirm electrolyte function under extreme applied potentials.

A significant difficulty in finding a good solid electrolyte is finding one that is stable at both the cathode and anode. From Figure 2, the $Li_7La_3Zr_2O_{12}$ garnet[5] and $LiAlO_2$ materials meet the stability requirements for high voltage cathodes. Because of its chemical similarity to $LiAlO_2$, ion exchanged Li β''-alumina also shows a wide stability window and with higher room temperature conductivity.[51] Incorporation of these oxide electrolytes into solid-state batteries is typically difficult, as many suffer from high grain boundary resistance or require high temperature sintering to obtain good contact with the electrodes. The binary halides have extraordinarily wide stability windows, but ionic conductivity is prohibitively low for all but the lowest power applications unless a second cation is added.[52−58] Unfortunately, the addition of such a cation typically makes these materials unstable against reduction by low voltage anodes (Figure 2).

Cathode coatings improve the performance of high voltage electrolytes by isolating the electrolyte materials from the low lithium potential, and imperfections in the coating allow reactions between cathode and electrolyte that yield passivating and ionically insulating reaction products. Because of this resilience to imperfections, thin coatings of lower conductivity materials can be used. Coating of the anode is in principle more difficult because lithium reduction of the electrolyte usually yields an electronically conductive (and therefore not passivating) decomposition product. One solution to this problem may be to combine two electrolytes in a single cell such that the high-voltage electrolyte protects the low-voltage electrolyte from oxidation, and the low-voltage electrolyte protects the other from reduction. Due to the thickness of the

DOI: 10.1021/acs.chemmater.5b04082
Chem. Mater. 2016, 28, 266−273

electrolyte vs a barrier coating, both materials need to have high ionic conductivity. One such solution would be to use a combination of Li_3PS_4 against the anode and Li_2MgCl_4 against the cathode. The Li_2MgCl_4 protects the Li_3PS_4 from oxidation by the cathode, and Li_3PS_4 protects the Li_2MgCl_4 from reduction by the anode. The most basic requirement for compatibility of the two electrolytes is that their μ_{Li} stability ranges overlap so there is no driving force for Li transfer between them, but they should also be chosen such that they do not react in other ways, which can be verified using the methodology of eq 2.

While complete thermodynamic stability of the bulk electrolyte and cathode phases in contact with each other is ideal, this is difficult to achieve, and our calculations show that this is likely not the case in a number of high performing systems. In batteries utilizing thiophosphate electrolytes our calculations show that the anode is likely to reduce the electrolyte, and in cells using a LiPON electrolyte we predict oxidation of nitrogen by the high cathode voltage. In both of these cases, the decomposition products are electronically insulating and have significant lithium concentration and so can support lithium ion conductivity. Optimization of the electrolyte/electrode combinations to produce similar passivating decomposition products may be a viable route toward creating high-performance systems and overcoming bulk chemical incompatibilities.

Our results suggest a few combinations of known cathode and electrolyte materials that may be combined to create high-performance batteries which have not been previously attempted. One such combination is that of Li_3PS_4 or the higher conductivity $Li_7P_3S_{11}$ glass-ceramic electrolyte combined with $LiVS_2$. This combination shows minimal decomposition energy according to Figure 4. This cell is expected to have a higher voltage and slightly better stability than the similar $LiTiS_2$ cathode with the $Li_2S-P_2S_5$ electrolyte of ref 46, which is also predicted by our calculations to have good performance, and was able to cycle for over 50 cycles without a barrier coating. Another possible combination predicted by our calculations is a $LiBH_4-LiTiS_2$ cell. $LiBH_4$ is unstable against the high voltage of $LiCoO_2$, and a steadily increasing interfacial resistance is seen experimentally[59] but is predicted to be more stable against the lower voltage $LiTiS_2$.

CONCLUSIONS

In this work, we have developed a computational method to screen cathode/electrolyte combinations for compatibility and interfacial stability in solid-state batteries. We find that the bulk material stability or passivation by ionically conductive products at the cathode μ_{Li} is essential for long-term device performance and that thermodynamic calculations allowing mass transfer across the interface are also required to provide a more thorough analysis of the interfacial reaction and better predict experimental results. We use our methodology to screen a wide range of electrolyte/electrode combinations, finding exceptionally good agreement with experimental results and also suggesting numerous novel cells with improved stabilities compared to current state-of-the-art. The breadth of our calculated data also serves as a valuable reference for experimentalists wishing to construct cells with new combinations of battery materials.

ASSOCIATED CONTENT

Supporting Information

The Supporting Information is available free of charge on the ACS Publications website at DOI: 10.1021/acs.chemmater.5b04082.

Details of calculated electrolyte anodic and cathodic reactions. Full list of calculated electrolyte decomposition reactions at cathode μ_{Li} and of reactions between cathode and electrolyte compositions (PDF)

AUTHOR INFORMATION

Corresponding Author

*E-mail: gceder@berkeley.edu.

Notes

The authors declare no competing financial interest.

ACKNOWLEDGMENTS

The authors thank the Samsung Advanced Institute of Technology for their funding of this research. This work used the Extreme Science and Engineering Discovery Environment (XSEDE), which is supported by National Science Foundation grant number ACI-1053575.

REFERENCES

(1) Li, J.; Ma, C.; Chi, M.; Liang, C.; Dudney, N. J. Solid Electrolyte: the Key for High-Voltage Lithium Batteries. *Adv. Energy Mater.* **2015**, *5*, 1401408.

(2) Khireddine, H.; Fabry, P.; Caneiro, A.; Bochu, B. Optimization of NASICON composition for Na^+ recognition. *Sens. Actuators, B* **1997**, *40*, 223−230.

(3) Fergus, J. W. Ion transport in sodium ion conducting solid electrolytes. *Solid State Ionics* **2012**, *227*, 102−112.

(4) Aono, H. Ionic Conductivity of Solid Electrolytes Based on Lithium Titanium Phosphate. *J. Electrochem. Soc.* **1990**, *137*, 1023−1027.

(5) Murugan, R.; Thangadurai, V.; Weppner, W. Fast lithium ion conduction in garnet-type $Li_7La_3Zr_2O_{12}$. *Angew. Chem., Int. Ed.* **2007**, *46*, 7778−7781.

(6) Ohta, S.; Kobayashi, T.; Asaoka, T. High lithium ionic conductivity in the garnet-type oxide $Li_{7-X}La_3(Zr_{2-X}, Nb_X)O_{12}$ (X = 0−2). *J. Power Sources* **2011**, *196*, 3342−3345.

(7) Allen, J.; Wolfenstine, J.; Rangasamy, E.; Sakamoto, J. Effect of substitution (Ta, Al, Ga) on the conductivity of $Li_7La_3Zr_2O_{12}$. *J. Power Sources* **2012**, *206*, 315−319.

(8) Thangadurai, V.; Narayanan, S.; Pinzaru, D. Garnet-type solid-state fast Li ion conductors for Li batteries: critical review. *Chem. Soc. Rev.* **2014**, *43*, 4714−4727.

(9) Ohta, S.; Seki, J.; Yagi, Y.; Kihira, Y.; Tani, T.; Asaoka, T. Co-sinterable lithium garnet-type oxide electrolyte with cathode for all-solid-state lithium ion battery. *J. Power Sources* **2014**, *265*, 40−44.

(10) Tatsumisago, M.; Nagao, M.; Hayashi, A. Recent development of sulfide solid electrolytes and interfacial modification for all-solid-state rechargeable lithium batteries. *J. Asian Ceram. Soc.* **2013**, *1*, 17−25.

(11) Hoshina, K.; Dokko, K.; Kanamura, K. Investigation on Electrochemical Interface between $Li_4Ti_5O_{12}$ and $Li_{1+x}Al_xTi_{2-x}(PO_4)_3$ NASICON-Type Solid Electrolyte. *J. Electrochem. Soc.* **2005**, *152*, A2138−A2142.

(12) Tachez, M.; Malugani, J.; Mercier, R.; Robert, G. Ionic conductivity of and phase transition in lithium thiophosphate Li_3PS_4. *Solid State Ionics* **1984**, *14*, 181−185.

(13) Kamaya, N.; Homma, K.; Yamakawa, Y.; Hirayama, M.; Kanno, R.; Yonemura, M.; Kamiyama, T.; Kato, Y.; Hama, S.; Kawamoto, K.; Mitsui, A. A lithium superionic conductor. *Nat. Mater.* **2011**, *10*, 682−686.

DOI: 10.1021/acs.chemmater.5b04082
Chem. Mater. 2016, 28, 266−273

(14) Seino, Y.; Ota, T.; Takada, K.; Hayashi, A.; Tatsumisago, M. A sulphide lithium super ion conductor is superior to liquid ion conductors for use in rechargeable batteries. *Energy Environ. Sci.* **2014**, *7*, 627−631.
(15) Ong, S. P.; Mo, Y.; Richards, W. D.; Miara, L.; Lee, H. S.; Ceder, G. Phase stability, electrochemical stability and ionic conductivity of the $Li_{10\pm1}MP_2X_{12}$ (M = Ge, Si, Sn, Al or P, and X = O, S or Se) family of superionic conductors. *Energy Environ. Sci.* **2013**, *6*, 148−156.
(16) Whiteley, J. M.; Woo, J. H.; Hu, E.; Nam, K.-W.; Lee, S.-H. Empowering the Lithium Metal Battery through a Silicon-Based Superionic Conductor. *J. Electrochem. Soc.* **2014**, *161*, A1812−A1817.
(17) Kuhn, A.; Duppel, V.; Lotsch, B. V. Tetragonal $Li_{10}GeP_2S_{12}$ and Li_7GePS_8 - exploring the Li ion dynamics in LGPS Li electrolytes. *Energy Environ. Sci.* **2013**, *6*, 3548−3552.
(18) Kuhn, A.; Gerbig, O.; Zhu, C.; Falkenberg, F.; Maier, J.; Lotsch, B. V. A new ultrafast superionic Li-conductor: ion dynamics in $Li_{11}Si_2PS_{12}$ and comparison with other tetragonal LGPS-type electrolytes. *Phys. Chem. Chem. Phys.* **2014**, *16*, 14669−14674.
(19) Bron, P.; Johansson, S.; Zick, K.; Schmedt auf der Günne, J.; Dehnen, S.; Roling, B. $Li_{10}SnP_2S_{12}$: an affordable lithium superionic conductor. *J. Am. Chem. Soc.* **2013**, *135*, 15694−15697.
(20) Takada, K.; Ohta, N.; Zhang, L.; Xu, X.; Hang, B. T.; Ohnishi, T.; Osada, M.; Sasaki, T. Interfacial phenomena in solid-state lithium battery with sulfide solid electrolyte. *Solid State Ionics* **2012**, *225*, 594−597.
(21) Takada, K. Progress and prospective of solid-state lithium batteries. *Acta Mater.* **2013**, *61*, 759−770.
(22) Takada, K.; Ohta, N.; Zhang, L.; Fukuda, K.; Sakaguchi, I.; Ma, R.; Osada, M.; Sasaki, T. Interfacial modification for high-power solid-state lithium batteries. *Solid State Ionics* **2008**, *179*, 1333−1337.
(23) Ohta, N.; Takada, K.; Zhang, L.; Ma, R.; Osada, M.; Sasaki, T. Enhancement of the High-Rate Capability of Solid-State Lithium Batteries by Nanoscale Interfacial Modification. *Adv. Mater.* **2006**, *18*, 2226−2229.
(24) Yu, X.; Bates, J.; Jellison, G.; Hart, F. A Stable Thin-Film Lithium Electrolyte: Lithium Phosphorus Oxynitride. *J. Electrochem. Soc.* **1997**, *144*, 524−532.
(25) McQuarrie, D. A. *Statistical Mechanics*; University Science Books: Sausalito, CA, 2000.
(26) Belsky, A.; Hellenbrandt, M.; Karen, V. L.; Luksch, P. New developments in the Inorganic Crystal Structure Database (ICSD): accessibility in support of materials research and design. *Acta Crystallogr., Sect. B: Struct. Sci.* **2002**, *58*, 364−369.
(27) Hautier, G.; Fischer, C. C.; Jain, A.; Mueller, T.; Ceder, G. Finding Natures Missing Ternary Oxide Compounds Using Machine Learning and Density Functional Theory. *Chem. Mater.* **2010**, *22*, 3762−3767.
(28) Jain, A.; Ong, S. P.; Hautier, G.; Chen, W.; Richards, W. D.; Dacek, S.; Cholia, S.; Gunter, D.; Skinner, D.; Ceder, G.; Persson, K. A. Commentary: The Materials Project: A materials genome approach to accelerating materials innovation. *APL Mater.* **2013**, *1*, 011002.
(29) Ong, S. P.; Wang, L.; Kang, B.; Ceder, G. Li-Fe-P-O_2 Phase Diagram from First Principles Calculations. *Chem. Mater.* **2008**, *20*, 1798−1807.
(30) Ong, S. P.; Richards, W. D.; Jain, A.; Hautier, G.; Kocher, M.; Cholia, S.; Gunter, D.; Chevrier, V. L.; Persson, K. A.; Ceder, G. Python Materials Genomics (pymatgen): A robust, open-source python library for materials analysis. *Comput. Mater. Sci.* **2013**, *68*, 314−319.
(31) Blöchl, P. E. Projector augmented-wave method. *Phys. Rev. B: Condens. Matter Mater. Phys.* **1994**, *50*, 17953−17979.
(32) Perdew, J. P.; Burke, K.; Ernzerhof, M. Generalized Gradient Approximation Made Simple. *Phys. Rev. Lett.* **1996**, *77*, 3865−3868.
(33) Kresse, G.; Furthmüller, J. Efficient iterative schemes for ab initio total-energy calculations using a plane-wave basis set. *Phys. Rev. B: Condens. Matter Mater. Phys.* **1996**, *54*, 11169−11186.
(34) Chase, M. W., Jr. NIST-JANAF Thermochemical Tables. *J. Phys. Chem. Ref. Data* **1998**.
(35) Kubaschewski, O.; Alcock, C. B.; Spencer, P. J. *Materials Thermochemistry*, 6th ed.; Pergamon Press: Oxford, 1993.
(36) Jain, A.; Hautier, G.; Ong, S. P.; Moore, C. J.; Fischer, C. C.; Persson, K. A.; Ceder, G. Formation enthalpies by mixing GGA and GGA + U calculations. *Phys. Rev. B: Condens. Matter Mater. Phys.* **2011**, *84*, 045115.
(37) Anisimov, V. I.; Zaanen, J.; Andersen, O. K. Band theory and Mott insulators: Hubbard U instead of Stoner I. *Phys. Rev. B: Condens. Matter Mater. Phys.* **1991**, *44*, 943−954.
(38) Dudarev, S. L.; Savrasov, S. Y.; Humphreys, C. J.; Sutton, A. P. Electron-energy-loss spectra and the structural stability of nickel oxide: An LSDA+U study. *Phys. Rev. B: Condens. Matter Mater. Phys.* **1998**, *57*, 1505−1509.
(39) Hautier, G.; Ong, S. P.; Jain, A.; Moore, C. J.; Ceder, G. Accuracy of density functional theory in predicting formation energies of ternary oxides from binary oxides and its implication on phase stability. *Phys. Rev. B: Condens. Matter Mater. Phys.* **2012**, *85*, 155208.
(40) Liu, Z.; Fu, W.; Payzant, E. A.; Yu, X.; Wu, Z.; Dudney, N. J.; Kiggans, J.; Hong, K.; Rondinone, A. J.; Liang, C. Anomalous high ionic conductivity of nanoporous β-Li_3PS_4. *J. Am. Chem. Soc.* **2013**, *135*, 975−978.
(41) Nazri, G. Preparation, structure and ionic conductivity of lithium phosphide. *Solid State Ionics* **1989**, *34*, 97−102.
(42) Schwöbel, A.; Hausbrand, R.; Jaegermann, W. Interface reactions between LiPON and lithium studied by in-situ X-ray photoemission. *Solid State Ionics* **2015**, *273*, 51−54.
(43) Senevirathne, K.; Day, C. S.; Gross, M. D.; Lachgar, A.; Holzwarth, N. A new crystalline LiPON electrolyte: Synthesis, properties, and electronic structure. *Solid State Ionics* **2013**, *233*, 95−101.
(44) Sahu, G.; Lin, Z.; Li, J.; Liu, Z.; Dudney, N.; Liang, C. Air-stable, high-conduction solid electrolytes of arsenic-substituted Li_4SnS_4. *Energy Environ. Sci.* **2014**, *7*, 1053−1058.
(45) Han, F.; Gao, T.; Zhu, Y.; Gaskell, K. J.; Wang, C. A Battery Made from a Single Material. *Adv. Mater.* **2015**, *27*, 3473−3483.
(46) Trevey, J. E.; Stoldt, C. R.; Lee, S.-H. High Power Nanocomposite TiS_2 Cathodes for All-Solid-State Lithium Batteries. *J. Electrochem. Soc.* **2011**, *158*, A1282−A1289.
(47) Dudney, N. J. Nanocrystalline $Li_xMn_{2-y}O_4$ Cathodes for Solid-State Thin-Film Rechargeable Lithium Batteries. *J. Electrochem. Soc.* **1999**, *146*, 2455−2464.
(48) Porter, D. A.; Easterling, K. E. *Phase Transformations in Metals and Alloys*, 2nd ed.; Nelson Thornes Ltd.: Cheltenham, United Kingdom, 1981.
(49) Sakuda, A.; Hayashi, A.; Tatsumisago, M. Interfacial Observation between $LiCoO_2$ Electrode and Li_2S-P_2S_5 Solid Electrolytes of All-Solid-State Lithium Secondary Batteries Using Transmission Electron Microscopy. *Chem. Mater.* **2010**, *22*, 949−956.
(50) Rangasamy, E.; Liu, Z.; Gobet, M.; Pilar, K.; Sahu, G.; Zhou, W.; Wu, H.; Greenbaum, S.; Liang, C. An Iodide-Based $Li_7P_2S_8I$ Superionic Conductor. *J. Am. Chem. Soc.* **2015**, *137*, 1384−1387.
(51) Briant, J.; Farrington, G. Ionic Conductivity in Lithium and Lithium Sodium Beta Alumina. *J. Electrochem. Soc.* **1981**, *128*, 1830−1834.
(52) Ginnings, D. C.; Phipps, T. E. Temperature-Conductance Curves of Solid Salts. III. Halides of Lithium. *J. Am. Chem. Soc.* **1930**, *52*, 1340−1345.
(53) Stoebe, T. G.; Huggins, R. A. Measurement of ionic diffusion in lithium fluoride by nuclear magnetic resonance techniques. *J. Mater. Sci.* **1966**, *1*, 117−126.
(54) Cros, C.; Hanebali, L.; Latie, L.; Villeneuve, G.; Gang, W. Structure, ionic motion and conductivity in some solid-solutions of the LiCl-MCl_2 systems (M = Mg,V,Mn). *Solid State Ionics* **1983**, *9−10*, 139−147.
(55) van Loon, C. J. J.; de Jong, J. Some chlorides with the inverse spinel structure. *Acta Crystallogr., Sect. B: Struct. Crystallogr. Cryst. Chem.* **1975**, *31*, 2549−2550.
(56) Weppner, W.; Huggins, R. A. Ionic conductivity of alkali metal chloroaluminates. *Phys. Lett. A* **1976**, *58*, 245−248.

DOI: 10.1021/acs.chemmater.5b04082
Chem. Mater. 2016, 28, 266−273

(57) Kanno, R.; Takeda, Y.; Yamamoto, O. Ionic conductivity of solid lithium ion conductors with the spinel structure: Li_2MCl_4 (M = Mg, Mn, Fe, Cd). *Mater. Res. Bull.* **1981**, *16*, 999−1005.
(58) Kanno, R.; Takeda, Y.; Yamamoto, O. Ionic Conductivity and Phase Transition of the Bromide Spinels, $Li_{2-2x}M_{1+x}Br_4$ (M = Mg, Mn). *J. Electrochem. Soc.* **1986**, *133*, 1052−1056.
(59) Takahashi, K.; Hattori, K.; Yamazaki, T.; Takada, K.; Matsuo, M.; Orimo, S.; Maekawa, H.; Takamura, H. All-solid-state lithium battery with $LiBH_4$ solid electrolyte. *J. Power Sources* **2013**, *226*, 61−64.

DOI: 10.1021/acs.chemmater.5b04082
Chem. Mater. 2016, 28, 266−273